Mon. Not. R. Astron. Soc. **000**, 000–000 (0000) Printed 5 February 2008 (MN LATEX style file v1.4)

ISOGAL Survey of Baade's Windows in the Mid-infrared

I.S. Glass[1], S. Ganesh[2,3], C. Alard[4], J.A.D.L. Blommaert[5], G. Gilmore[6], T. Lloyd Evans[1], A. Omont[2], M. Schultheis[2] and G. Simon[4]

[1] *South African Astronomical Observatory, PO Box 9, Observatory 7935, South Africa*
[2] *Institut d'Astrophysique de Paris, CNRS, 98bis Blvd Arago, Paris F75014, France*
[3] *on leave from Physical Research Laboratory, Navarangpura, Ahmedabad 380009, India*
[4] *DASGAL, UMR CNRS N◦ 335, Observatoire de Paris, 21 Avenue de l'Observatoire, Paris F75014, France*
[5] *ISO Data Centre, Astrophysics Div., Space Science Dept. of ESA, Apartado 50727, Madrid E28080, Spain*
[6] *Institute of Astronomy, The Observatories, Madingley Rd., Cambridge CB3 0HA, UK*

arXiv:astro-ph/9904010v1 1 Apr 1999

Sent to MNRAS 22 Jan 1999

ABSTRACT

The ISOGAL mid-infrared survey of areas close to the Galactic Plane aims to determine their stellar content and its possible bearing on the history of the Galaxy. The NGC 6522 and Sgr I Baade's Windows of low obscuration towards the inner parts of the Bulge represent ideal places in which to calibrate and understand the ISOGAL colour-magnitude diagrams, which are more difficult to interpret in heavily reddened fields.

The survey observations were made with the ISOCAM instrument of the ISO satellite. The filter bands chosen were LW2 ($\sim$7 μm) and LW3 ($\sim$15 μm).

The results presented here show that most of the detected objects are late M-type giants on the AGB, with a cut-off for those earlier than M3–M4. The most luminous members of these two Bulge fields at 7 μm are the Mira variables. However, it is evident that they represent the end of a sequence of increasing 15 μm dust emission which commences with M giants of earlier sub-type.

In observations of late-type giants the ISOCAM 15 μm band is mainly sensitive to the cool silicate or aluminate dust shells which overwhelm the photospheric emission. However, in ordinary M-giant stars, the 7 μm band is not strongly affected by dust emission and may be influenced instead by absorption. The ν_2 band of water at 6.25 μm and the SiO fundamental at 7.9 μm are likely contributors to this effect. Miras are more luminous at 7 μm and have redder K_0–[7] colours than other M giants. Their [7]–[15] colours are consequently bluer than might be expected by extrapolating from warmer M-giants.

A group of late M stars has been found which vary little or not at all but have infrared colours typical of well-developed dust shells. Their luminosities are similar to those of 200–300 day Miras but they have slightly redder [7]–[15] colours which form an extension of the ordinary M giant sequence. They may belong to the class of red semi-regular variables.

The Mira dust shells show a mid-infrared [7]–[15] colour-period relation.

In these two fields there is no component of high-luminosity late-type variables obscured at K and shorter wavelengths such as is seen in the Magellanic Clouds. The upper limit of LPV periods in these fields remains at *ca* 700 days.

Key words: Stars: AGB, Stars:variables:others, Galaxy:center, Galaxy: stellar content

1 INTRODUCTION

The ISOGAL* (Pérault et al, 1996; Ojha, Omont and Simon, 1997, Omont et al, 1999 a,b,c) project has surveyed

© 0000 RAS

* This is paper no. 3 in a refereed journal based on data from the ISOGAL project.

a number of fields at low galactic latitude in the intermediate infrared using the ISOCAM (Cesarsky et al., 1996) instrument of the ISO† satellite. Its aim is the better understanding of the stellar content of the inner Galaxy, mostly in very obscured regions. Normally, the filter bands chosen for the observations were LW2 (5.5–8 μm) and LW3 (12–18 μm). The pixel size was 6×6 arcsec^2.

The dusty shells surrounding mass-losing late-type stars are expected to be particularly prevalent amongst the objects that should be detected. These stars will also, in general, be seen by the DENIS and 2-MASS surveys at IJK$_S$ and JHK$_S$ respectively.

However, in the more obscured ISOGAL fields, there is little information available concerning individual stars except for those few that are among the most luminous OH/IR sources. For this reason, it was decided to include some of the relatively unobscured fields known as "Baade's Windows", located in the inner Bulge, in the programme. These should serve as relatively well surveyed comparison areas. A_V is thought to average 1.78 ± 0.10 mag in these fields as a whole (see Glass et al, 1995)‡. In both cases it will be almost negligible in the LW2 and LW3 bands discussed here and the ISOGAL magnitudes have not been corrected for interstellar extinction.

In particular, we have examined the field located around the globular cluster NGC 6522 and that known as Sgr I. The late-type stellar contents (M-stars) of the first of these fields have been surveyed and classified by Blanco, McCarthy and Blanco (1984) (BMB) by objective prism, and a smaller portion has been examined similarly by Blanco (1986) to fainter magnitudes. I-band photometry is given for the BMB survey, together with an indication of variability, whereas V-band photometry is provided by Blanco (1986). The long-period variable star content of both fields has been surveyed by Lloyd Evans (1976; TLE), using I-band plates, and he summarizes previous work at visible wavelengths.

Infrared ($JHKL$) studies of Lloyd Evans' variable stars in NGC 6522 and Sgr I were carried out by Glass and Feast (1982) in order to make use of their period-luminosity relation for determining the distance to the Galactic Centre. It was later pointed out by Feast (1985) that many of the IRAS sources in the Sgr I and NGC 6522 windows could be identified with known variables. These were listed by Glass (1986) who showed that the remaining (unidentified) IRAS sources in Sgr I were very red at $JHKL$ and were also likely to be long-period variables. Following this work, the known long-period variables and IRAS sources in the Sgr I field were monitored by Glass et al (1995) and periods were confirmed or determined for all sources except one that was non-variable. The $K_0, (H-K)_0$ colour-magnitude diagram of the Sgr I field shows that the long-period variables are among the reddest and most luminous objects (Glass, 1993) at these wavelengths. The dispersion of the K_0, $\log P$ relation in Sgr I is quite small (~ 0.35 mag; Glass et al., 1995). This implies that most of the AGB stars in the field are at a nearly uniform distance, allowing a simple connection to be made between apparent and absolute magnitudes.

Photometry of some of the BMB (1984) stars has been obtained by Frogel and Whitford (1987). Deep near-infrared photometry of the NGC 6522 window is presented by Tiede, Frogel and Terndrup (1995). The DENIS results will form the subject of a separate paper.

Table 1. Journal of observations

Field	Filter	Identification	Julian date
NGC 6522	LW2	47101493	2450509
NGC 6522	LW2	84001115	2450877
NGC 6522	LW3	84001116	2450877
Sgr I	LW2	47101494	2450509
Sgr I	LW2	83800913	2450875
Sgr I	LW3	83800914	2450875

2 ISOGAL OBSERVATIONS

The ISOGAL observations were made in the two filters mentioned, as rasters covering squares of 15×15 arcmin^2 orientated in ℓ,b. They were centered at ℓ=+1.03°, b=–3.83°, which includes the globular cluster NGC 6522 itself, and at ℓ=+1.37°, b=–2.63° in Sgr I. Each position on the sky was observed for a total of 22s on average.

Two rasters of each field were made with the LW2 filter and one with LW3 (Table 1). The first three digits of each identification indicate the ISO revolution number ($\simeq$ day of flight). The second LW2 observation in each case is almost simultaneous with that in LW3 (within ~ 30 min). The images are shown in Figs 1–4. The 6″ pixel field of view was utilised in all cases.

Reduction of the science processed data (SPD) from version 6.32 of the OLP (Off-line Processing) pipeline was carried out with the CIA§ package (CIA version 3.0) The data were first corrected for dark current, using the default method of subtracting a 'model' dark frame. Following this, the cosmic-ray hits were removed from the data cube using the multi-resolution median method. At this stage, two copies of the data cube were made and the individual copies were treated by two different methods for simulating the time behaviour of the pixels of the ISOCAM detectors: the 'vision' method and the 'IAS model transient correction', also known as the 'inversion' method (Abergel et al., 1998). The vision method does not correct much for the transient behaviour but is useful in removing the memory remnants (electronic ghosts) of previously observed strong sources. From this stage onwards in the reduction procedure we thus had two sets of data, corresponding to the two methods of stabilization. For each data set the images at each raster

† ISO is an ESA project with instruments funded by ESA member states (especially the PI countries: France, Germany, the Netherlands and the United Kingdom) and with the participation of ISAS and NASA.

‡ An extinction map by Stanek (1996) indicates, however, that it is particularly low (about $A_V \sim 1.45$) in the part of the NGC 6522 window covered by our observations. The K_0 magnitudes that we quote later in this work remain as published by the original authors, who used $A_K \sim 0.14$ mag.

§ The ISOCAM data presented in this paper was analysed using 'CIA', a joint development by the ESA Astrophysics Division and the ISOCAM Consortium. The ISOCAM Consortium is led by the ISOCAM PI, C. Cesarsky, Direction des Sciences de la Matière, C.E.A., France.

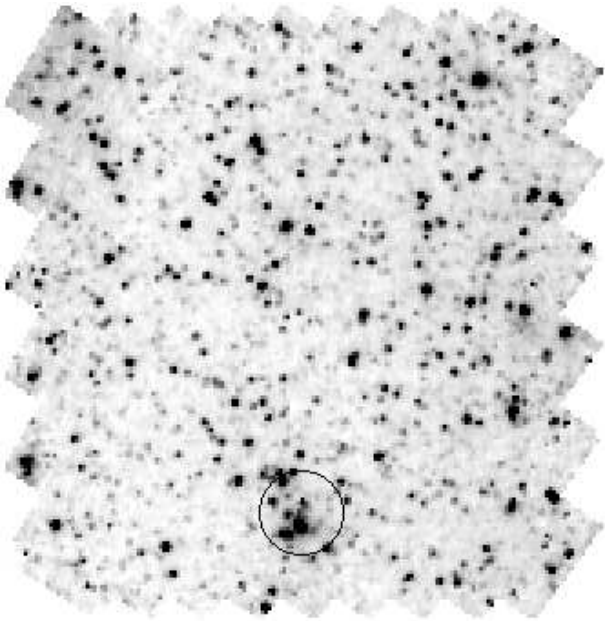

Figure 1. ISOCAM 7 μm (LW2) image of the field in the NGC 6522 Baade Window, covering 15 × 15 arcmin^2. Increasing ℓ is to the left and increasing b is upwards. The NGC 6522 cluster is visible near the middle of the bottom edge (Image 84001115). The circle has a radius 0.02°.

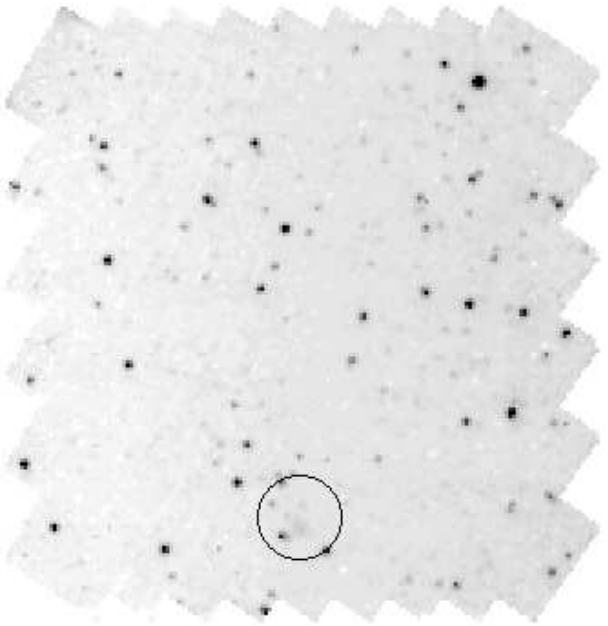

Figure 2. ISOCAM 15 μm (LW3) image of the field in the NGC 6522 Baade Window, covering 15 × 15 arcmin^2. Increasing ℓ is to the left and increasing b is upwards (Image 84001116).

pointing were averaged. The data were then flat-fielded with the flats generated from the raster observations themselves. Subsequent to the flat fielding, the individual images were mosaiced together after correcting for the field of view distortion using the 'projection' method.

The two individual rasters thus obtained were then in

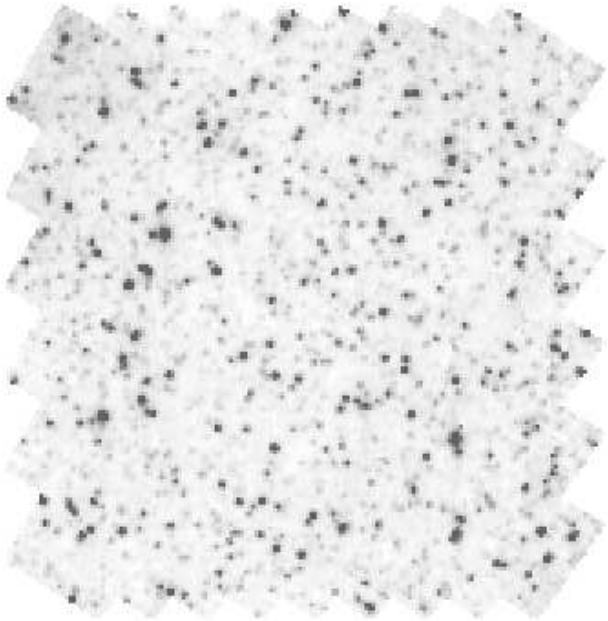

Figure 3. ISOCAM 7 μm (LW2) image of the field in the Sgr I Baade Window, covering 15 × 15 arcmin^2. Increasing ℓ is to the left and increasing b is upwards (Image 83800913).

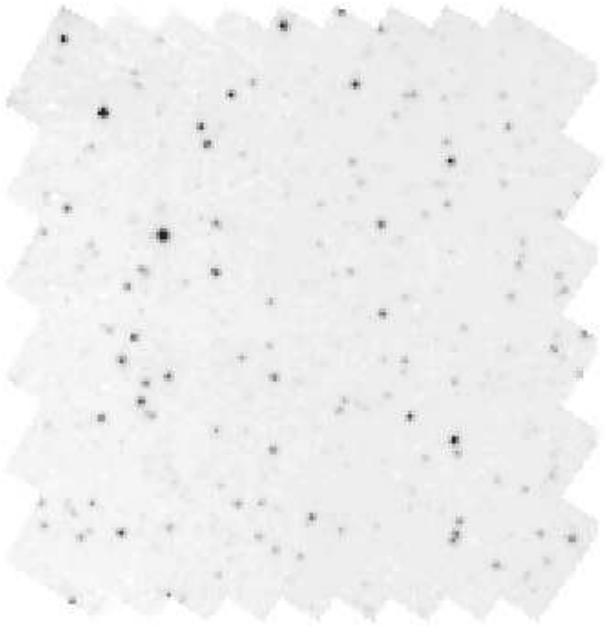

Figure 4. ISOCAM 15 μm (LW3) image of the field in the Sgr I Baade Window, covering 15 × 15 arcmin^2. Increasing ℓ is to the left and increasing b is upwards (Image 83800914).

units of ADU/gain/sec. They were converted into mJy/pixel units within CIA. The conversion factors were:

$F(\mathrm{mJy}) = (\mathrm{ADU/gain/sec})/2.33$

for LW2 and

$F(\mathrm{mJy}) = (\mathrm{ADU/gain/sec})/1.97.$

for LW3 (Blommaert, 1998).

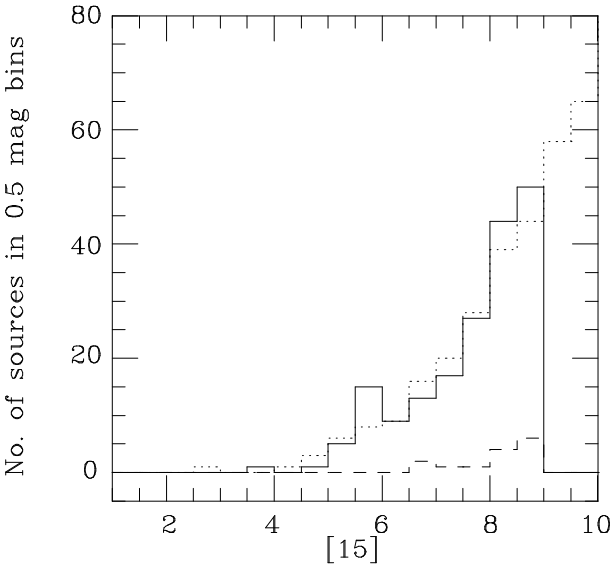

Figure 5. Total observed (solid line) and expected (dotted line) distributions of all sources at 15 μm (LW3) in the NGC 6522 field, demonstrating that the LW3 detections are reliable to $\sim$ 9.0 mag (see text for explanation). The dashed histogram is the distribution of sources detected only at 15 μm. The latter may be spurious, especially near the faint limit.

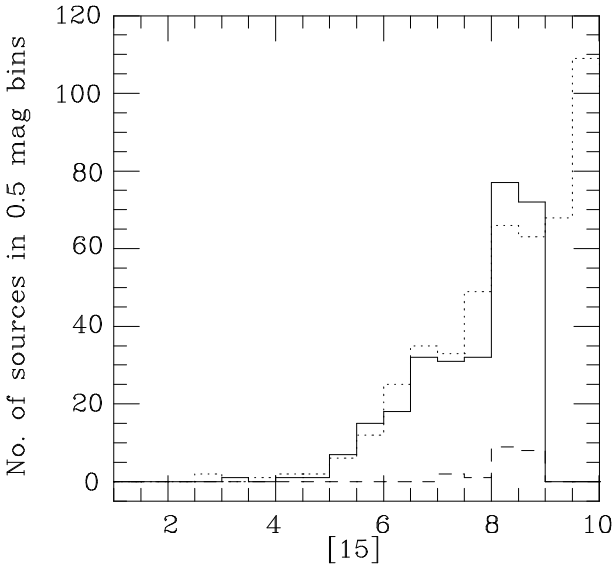

Figure 6. Observed (solid line) and expected (dotted line) distributions for the Sgr I field. See caption of Fig. 5 for further details.

These are correct for a $F_\lambda \propto \lambda^{-1}$ power-law spectrum at wavelengths 6.7 μm and 14.3 μm respectively.

Source extraction was performed on each pair of reduced images using a point spread function fitting routine (Alard et al., in preparation). The vision-treated point sources were cross-identified with the inversion-treated ones and the final catalogue of point sources was built with the inversion photometry for those sources found in both vision- and inversion-treated images. This procedure ensured that most false sources were dropped while the better photometry of the inversion-treated images was retained.

Conversion to magnitudes was then carried out using the formulae

$$[7] = 12.38 - 2.5 \log F_{\rm LW2}({\rm mJy})$$

and

$$[15] = 10.79 - 2.5 \log F_{\rm LW3}({\rm mJy})$$

where the zero point has been chosen to get zero magnitude for a Vega model flux at the respective wavelengths mentioned earlier. We have limited the extracted catalogue to sources with fluxes greater than 5mJy in both LW2 and LW3. This corresponds to [7] = 10.64 and [15] = 8.99.

The reliability of the ISOCAM data is affected at the faint end by crowding and noise. These effects can be investigated by constructing histograms of source counts vs mag. Figure 5 is a histogram of the LW3 observations in the NGC 6522 field. Also included is the expected distribution, based on averaged [7] magnitudes and a relation $[15]_{\rm expected} = 1.56 \times [7] - 5.0$ (This approximation is a line passing through the [15], [7]–[15] values of (9.0, 0.0) and (3.96, 1.8) in the colour-magnitude diagrams (Figures 8 and 9)). It appears that the NGC 6522 detections at 15 μm are reliable to a depth of [15] $\sim$ 9.0 mag. Figure 6 is a similar diagram for the Sgr I field.

From analysis of repeated observations, the rms dispersion of the ISOGAL photometry is estimated to be generally less than 0.2 magnitudes, except towards the fainter magnitude ranges, where it rises to $\sim$0.4 mag (Ganesh et al., in preparation). See also section 3.3.3 of this paper. A small uncertainty remains in the absolute photometry due to the crowded nature of the ISOGAL fields. It is felt that the behaviour of the inversion method of transient correction is not yet completely understood and it is hoped that the uncertainty can be reduced in the near future.

It may be noted that, with $\sim$ 45 and $\sim$ 35 pixels per LW2 source, respectively, the density of sources in our two fields is close to the confusion limit in both.

The astrometry of the extracted sources was improved by using the newly available DENIS K band observations of these fields. A systematic shift of 0.8″ (with a rms dispersion of 0.6″) in right ascension and 5.1″ (0.7″) in declination was found for the NGC 6522 observation. The corresponding numbers for the Sgr I observation were found to be 2.0″ (0.9″) and 6.1″ (0.8″) respectively. The positions given in Tables 2 and 3 include the corrections.

2.1 NGC 6522

Sources were extracted from the LW2 and LW3 images and cross-correlated to form a working table. The total number detected was 497. Of these, 182 or 37% were detected at 15 μm. The remainder were detected only in LW2, usually because they were too faint to be seen at 15 μm. Sources were detected in both LW2 exposures in 363 cases. Non-detections in LW2 are often clearly due to blending with strong sources in their neighbourhoods. In some cases the reliability of the detection is questionable and needs to be confirmed when deeper data become available. Fifty-four sources were detected only in the first LW2 observation and 66 only in the second. These are for the most part close to the detection limit and their existence requires confirmation.

Some 14 sources were detected at 15 μm only. Each was

investigated visually in the three images and comments on individual sources were included in the working table.

Because of the small uncertainty in the zero-point of the photometry that has already been mentioned, we have decided to publish only those sources with [7] ≤ 7.5 for the time being (see table 2). The full table will be published when it is felt that the performance of the camera in crowded fields is better understood.

The lack of a strong density enhancement in the neighbourhood of NGC 6522 indicates that few sources are likely to be members of the cluster itself. Circles with radius 0.02 degree about the cluster centre are shown on figs. 1 and 2.

2.2 Sgr I

A total of 696 sources were detected. Of these, 287 or 41% were detected at 15 μm . Only 20 sources were detected solely at 15 μm. At 7 μm, 517 sources were detected twice. Eighty-eight sources were only seen in the first LW2 exposure and 71 were only seen in the second. As in the case of the NGC 6522 field, only those sources with [7] ≤ 7.5 are given in Table 3.

3 CORRELATIONS WITH OTHER CATALOGUES

The fields observed by ISOGAL overlap completely or in part with areas surveyed in other ways.

3.1 Spectroscopic information (NGC 6522 only)

The spectroscopic survey of BMB (1984) covers M6 and later M-type giants. Spatially, more than 80% of our field is included and almost all their stars in the overlap area ($\sim$ 112) were detected. Cross-correlation of source positions was performed by means of transparent overlays. The sources BMB20 and 21 may both correspond to our no. 118. The following BMB sources that we do *not* detect are of spectral type M6: BMB 41, 56, 62, 82, 100, and 118. We also did not see BMB 13 (M5). These are all at the early end of the range.

More interesting is the deeper survey of Blanco (1986) which covers a much smaller portion of the ISOGAL field but includes earlier spectral types, from M1 onwards. Table 4 summarizes our detections as a function of spectral type for the part of the field coincident with the deep spectroscopic survey. It is clear that our survey cuts off between spectral classes M3 and M4 (III), where the changeover from majority non-detections to majority detections occurs.

It must also be expected that some brighter objects from the foreground will have been included. In fact, there are eight objects in the overlap region that were detected in the ISOGAL programme but were not classified as having spectra in the range M1–M9 by Blanco (1986). Their I-band counterparts appear quite bright. They were examined on I and V plates (Lloyd Evans, 1976) and were found to be probably non-variable and to have colours corresponding to K or early M types. Only one was detected at 15 μm. The others are almost certainly foreground stars.

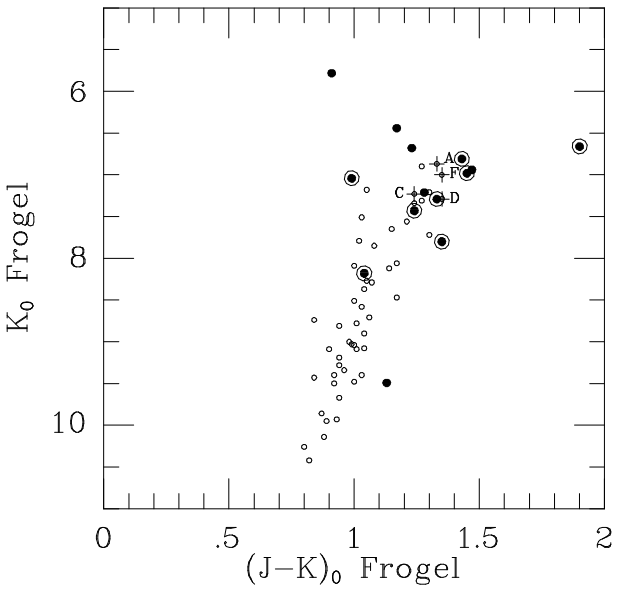

Figure 7. $(J-K)_0$, K_0 diagram for ISOGAL objects in the NGC 6522 field that have photometry by Frogel and Whitford (1987) or Tiede, Frogel and Terndrup (1995) on the CIT/CTIO system. The NGC 6522 Miras are indicated by heavy points. Other high mass-loss objects specially examined (see below, section 6) are crossed. Also shown as circled points are Miras in our Sgr I field, taken from Glass et al. (1995). The tip of the RGB is estimated to occur at $K \sim 8.2$. Note that the NGC 6522 Mira brightest at K (= TLE D9) appears unusually blue in the Frogel and Whitford photometry. It was considerably redder when measured by Glass and Feast (1982).

3.2 Photometric information

3.2.1 NGC 6522

Only one object in the IRAS Point-source Catalog falls within our survey area. This is IRAS 17598-2957, which coincides with our no. 180, and has [15] = 5.11 (IRAS 12 μm flux = 0.87 Jy). Star 224 has [15] = 4.82 and star 12 has [15] = 3.64, so it is surprising that these objects were not also detected by IRAS. The cause may be variability or crowding of sources.

A number (56) of our NGC 6522 stars have been observed by Frogel and Whitford (1987) or Tiede, Frogel and Terndrup (1995) on the CTIO/CIT near-infrared system. Some of the variables also have photometry by Glass and Feast (1982). Fig. 7 shows the $(J-K)_0$, K_0 diagram of the ISOGAL objects that were measured on the CIT/CTIO system.

I-band photographic photometry was included in the BMB (1984) M-star survey. Sharples, Walker and Cropper (1990) have pointed out that the stars with I mag < 11.8 have a significantly lower velocity dispersion than fainter ones, indicating that they probably belong to the foreground disc. A similar effect is seen amongst K giants in the same field (Sadler, Terndrup and Rich, 1996). There are 9 BMB stars with $I < 11.8$ amongst the ISO detections, including two Miras (TLE 238 and TLE 136) and a possible semiregular variable (BMB 18).

Table 2. Bright sources detected by ISO in the NGC 6522 field

No.	Name	[7]#1	[7]#2	$[7]_{avg}$	[15]	Cross-identifications and comments.
1	ISOGAL-PJ180228.2-300038	6.75		6.75		near raster edge - poor astrometry
12	ISOGAL-PJ180234.8-295957	4.88	5.05	4.96	3.64	TLED9 400:d GF FW
14	ISOGAL-PJ180235.2-295855	6.46	6.53	6.50	5.78	*H
26	ISOGAL-PJ180239.4-295636	7.46		7.46	7.16	
41	ISOGAL-PJ180242.9-300335		7.48	7.48	5.86	
46	ISOGAL-PJ180243.5-300250	6.77	6.56	6.66	6.35	Unresolved? (See 49)
85	ISOGAL-PJ180251.2-300013	7.59	7.39	7.49	6.61	BMB7 7
110	ISOGAL-PJ180256.1-295533	6.77	6.64	6.71	5.77	*I
120	ISOGAL-PJ180257.0-300417	6.23	6.76	6.50	5.54	*G BMB18 6
128	ISOGAL-PJ180257.6-295124	6.95	6.65	6.80	6.32	
147	ISOGAL-PJ180259.6-300253	6.92	7.13	7.03	5.28	*C BMB28 7 FW
162	ISOGAL-PJ180301.1-300141	6.23	6.49	6.36	5.51	*B
170	ISOGAL-PJ180302.3-295806	7.18	7.23	7.21	7.04	
180	ISOGAL-PJ180303.4-295729	6.03	6.03	6.03	5.11	TLE 228 270d GF (3) BMB39 9 150
192	ISOGAL-PJ180305.3-295515	6.84	6.87	6.86	5.52	*F BMB46 7 FW (Unresolved in LW2?)
205	ISOGAL-PJ180306.3-295203	7.50	7.31	7.40	5.75	
218	ISOGAL-PJ180307.8-300034	7.26	7.16	7.21	5.84	BMB52 9 FW
224	ISOGAL-PJ180308.5-300524	6.39	6.25	6.32	4.82	TLE 403 335d GF BMB54 7 FW
235	ISOGAL-PJ180309.8-295505	7.23	7.35	7.29	7.01	BMB61 7
245	ISOGAL-PJ180311.5-295745	6.75	6.93	6.84	5.80	TLE 238 290: (2) BMB63 7 FW
254	ISOGAL-PJ180312.5-300428	6.99	7.10	7.04	5.98	BMB64 7
256	ISOGAL-PJ180313.4-300055	7.42	7.33	7.38	6.35	BMB67 8
270	ISOGAL-PJ180315.5-300737	7.42	7.25	7.33	6.57	BMB70 6.5 - at edge in LW2 (unresolved?)
299	ISOGAL-PJ180318.4-295346	7.23	7.07	7.15	5.29	*D BMB86 9 FW
333	ISOGAL-PJ180322.4-300255	7.43	7.43	7.43	7.08	B24 M6 BMB93 6 FW
382	ISOGAL-PJ180328.4-295544	7.34	7.17	7.25	5.54	*E BMB119 9 (unresolved?)
389	ISOGAL-PJ180329.4-295939	7.36	7.40	7.38	5.99	B57 M7 BMB120 7 FW
410	ISOGAL-PJ180331.3-300100	6.77	6.65	6.71	6.33	BMB129 6.5 GC member?
432	ISOGAL-PJ180334.1-295957	7.03	6.92	6.97	5.56	B81 M8 BMB142 8 FW
441	ISOGAL-PJ180335.7-300300	7.33	7.45	7.39	5.74	GC member?
445	ISOGAL-PJ180336.9-300147	7.12	7.02	7.07	6.03	BMB152 9 V (Unresolved?) GC member?
476	ISOGAL-PJ180346.1-295911	6.91	7.08	7.00	5.21	*A B138 M7 BMB179 7 FW
491	ISOGAL-PJ180350.9-295617	6.29	6.33	6.31	5.26	TLE136 270d (1) BMB194 6.5 FW

Notes to tables 2 and 3:
The "Name" column follows the IAU nomenclature. The letter "P" denotes provisional
1 Noted by Lloyd Evans (1976) as semiregular
2 Noted by Lloyd Evans (1976) as small amplitude in I
3 =IRAS 17598-2957

Key:
TLE: LPVs in Lloyd Evans (1976)
GF: Miras with $JHKL$ photometry by Glass and Feast (1982)
A etc: stars selected for blink examination
B: Stars classified by Blanco (1986)
BMB: stars classified by BMB (1984), followed by M sub-class
FW: JHK photometry in Frogel & Whitford (1987)

3.2.2 Sgr I

There are two IRAS sources within the ISOGAL field, viz no. 363 = IRAS 17559-2901 = TLE 53 (IRAS 12 μm flux = 1.7 Jy) and no. 247 = IRAS 17558-2858 = TLE 79 (IRAS 12 μm flux = 1.19 Jy).

3.3 Mira-type Variability

The spectra of Mira variables change by several sub-types around the cycle, so that a direct correspondence between, for example, period and spectral sub-type is not to be expected.

As will be seen, several stars with positions around those of the less-luminous Miras in the colour-magnitude diagrams have been examined for large-amplitude variability with negative results. It therefore appears that our inventory of the Mira variables in these two fields is complete.

3.3.1 NGC 6522

Six stars from the ISOGAL field were detected by Lloyd Evans (1976) as Mira variables. Four of these are amongst the most luminous at 15 μm, while one, of relatively short period for a "long-period variable" is near the limit of detection. The IRAS source corresponds to TLE 228. Table 5 shows the cross-identifications. The relatively short-period star (115d) TLE 395 is only just detectable at 15 μm.

The two ISOGAL 7 μm exposures were compared by magnitude range (in the first measurement) and the average

Table 3. Bright sources detected in the Sgr I field by ISO

No	Name	[7]#1	[7]#2	$[7]_{avg}$	[15]	Cross-identifications and comments
32	ISOGAL-PJ175836.4-290802	7.27	7.14	7.21	6.28	
45	ISOGAL-PJ175839.1-290522	7.29	7.23	7.26	6.54	
61	ISOGAL-PJ175841.8-290352	6.84	6.88	6.86	5.41	*D
65	ISOGAL-PJ175842.0-290649	7.19	7.06	7.12	6.73	Unresolved?
69	ISOGAL-PJ175842.6-291028		7.44	7.44	6.59	at edge of raster; outside [7]#1 observation; unresolved?
78	ISOGAL-PJ175843.9-290711	6.61	6.06	6.33	5.28	TLE65 Unresolved?
112	ISOGAL-PJ175848.0-291002	7.32	7.34	7.33	7.26	
117	ISOGAL-PJ175848.7-290743	7.41	7.55	7.48	6.58	
129	ISOGAL-PJ175850.3-290454	7.43	7.52	7.47	6.57	
167	ISOGAL-PJ175854.8-285831	6.93	6.76	6.84	6.94	
168	ISOGAL-PJ175854.9-290117	7.40	7.53	7.46	7.76	
170	ISOGAL-PJ175855.1-290627	6.95	7.03	6.99	5.53	*M Unresolved?
180	ISOGAL-PJ175855.9-285845	7.34	7.42	7.38	6.86	
187	ISOGAL-PJ175856.4-290049	6.81	6.65	6.73	5.37	*F
189	ISOGAL-PJ175856.6-290213	7.30	7.35	7.32	7.24	
200	ISOGAL-PJ175857.4-291215	7.14	7.25	7.20	6.11	
206	ISOGAL-PJ175857.8-290114	6.60	6.71	6.65	5.34	*J
247	ISOGAL-PJ175901.1-285821	6.13	5.79	5.96	4.46	TLE79 Unresolved?
291	ISOGAL-PJ175904.7-290744	7.01	7.03	7.02	5.65	*N
303	ISOGAL-PJ175905.7-290235	6.99	7.17	7.08	6.01	
328	ISOGAL-PJ175907.3-291024	7.17	7.31	7.24	6.68	
338	ISOGAL-PJ175908.3-290855	7.53	7.38	7.46	6.40	
351	ISOGAL-PJ175909.5-290903	7.34	7.40	7.37	7.27	
352	ISOGAL-PJ175909.5-290825	7.52	7.45	7.48	7.31	
363	ISOGAL-PJ175910.5-290129	4.66	5.08	4.87	3.37	TLE53 Unresolved?
365	ISOGAL-PJ175910.6-290456	7.22	7.27	7.24	6.45	
375	ISOGAL-PJ175911.1-290315	6.66	6.75	6.71	5.34	*E Unresolved?
400	ISOGAL-PJ175913.6-285812	7.37	7.34	7.36	7.10	
401	ISOGAL-PJ175913.7-291113	5.03	4.97	5.00	4.77	
402	ISOGAL-PJ175913.7-285852	7.04	6.88	6.96	5.75	TLE87
405	ISOGAL-PJ175914.0-290950	7.24	7.05	7.14	5.58	*G
410	ISOGAL-PJ175914.4-291335	7.24	7.18	7.21	6.80	
416	ISOGAL-PJ175914.8-291129	7.46	7.35	7.40	6.41	
421	ISOGAL-PJ175915.5-290133	6.79	6.82	6.80	6.07	appears unresolved.
434	ISOGAL-PJ175916.8-290010	7.27	7.22	7.24	7.38	
446	ISOGAL-PJ175917.7-285839	7.47	7.40	7.44		
452	ISOGAL-PJ175918.2-291433	6.69	6.63	6.66	6.50	
453	ISOGAL-PJ175918.2-290123	5.99	6.15	6.07	5.83	
455	ISOGAL-PJ175918.5-290504	7.34	7.25	7.29	6.58	
457	ISOGAL-PJ175918.5-290607	7.28	7.36	7.32	5.77	
478	ISOGAL-PJ175920.7-291505	7.41	7.33	7.37	7.07	
488	ISOGAL-PJ175922.0-291229	6.36	6.55	6.46	6.03	
511	ISOGAL-PJ175923.4-290215	6.18	6.56	6.37	5.39	TLE54
514	ISOGAL-PJ175923.7-291236	6.76	6.91	6.83	5.64	TLE39
522	ISOGAL-PJ175924.4-291358	7.24	7.24	7.24	6.21	
524	ISOGAL-PJ175924.6-291236		7.47	7.47	6.15	
529	ISOGAL-PJ175925.3-290336	7.05	7.22	7.13	5.70	*L
540	ISOGAL-PJ175926.4-290707	7.15	6.90	7.03	5.84	
541	ISOGAL-PJ175926.5-290217	7.31	7.37	7.34	5.60	*H
550	ISOGAL-PJ175927.4-290309	7.75	7.17	7.46	5.91	
556	ISOGAL-PJ175927.9-290530	7.44	7.47	7.46	6.61	
576	ISOGAL-PJ175929.7-290318	6.35	6.68	6.51	5.47	TLE55
581	ISOGAL-PJ175930.7-290950	6.77	7.00	6.88	6.83	
585	ISOGAL-PJ175931.1-290858	6.93	7.18	7.05	5.67	*K
601	ISOGAL-PJ175932.8-290734	7.25	7.33	7.29	6.59	
609	ISOGAL-PJ175934.0-290236	5.41	5.63	5.52	5.53	unresolved?
613	ISOGAL-PJ175934.4-290702	7.43	7.49	7.46	6.40	
626	ISOGAL-PJ175936.1-290915	6.94	6.97	6.96	6.75	
633	ISOGAL-PJ175937.0-290834	7.38	7.50	7.44	6.56	
681	ISOGAL-PJ175945.2-290442	6.99	7.26	7.12	5.54	*C
684	ISOGAL-PJ175946.1-290318	7.03	7.44	7.24	6.97	TLE57 Unresolved?
686	ISOGAL-PJ175947.0-290227	7.27		7.27		at edge of raster
689	ISOGAL-PJ175948.2-290350	6.90	7.21	7.05	6.37	TLE56
692	ISOGAL-PJ175949.3-290247	7.36	7.48	7.42		

Table 4. ISOGAL detections in NGC 6522 as a function of spectral type for stars classified in a deep objective-prism survey by Blanco (1986), falling within the area of mutual overlap.

M class	Detected	Not detected
1	0	38
2	5	15
3	7	9
4	6	5
5	6	2
6	13	0
6.5	6	0
7	5	0
8	1	0

Table 5. Stars within the ISOGAL NGC 6522 field known to be long-period variables

ISOGAL no.	Lloyd Evans no.	Period days	Differences[1]
12	D9	400:	-0.17
180[2]	228	270	0.00
224	403	335	0.14
245	238	290:	-0.18
258	395	115	0.27
491	136	270	-0.04

Note: A colon denotes uncertainty in the period
[1]Between the two measurements in LW2. See also table 6.
[2] = IRAS 17598-2957

differences and their rms values were found for stars that appear in both. The result is shown in Table 6.

3.3.2 Sgr I

Nine stars within the ISOGAL field are known long-period variables (see Table 7). These have been followed at *JHKL* by Glass et al (1995), who list their mean magnitudes and periods.

The two ISOGAL 7 μm exposures were again compared by magnitude range. The result is shown in Table 8.

3.3.3 Photometric consistency

If the known variables are omitted the average and rms differences are somewhat reduced. In the case of NGC 6522, the known variables show only small differences and do not materially affect the rms values.

The error in the repeatibility of a single 7 μm observation in either field is thus about 0.14 mag, where we have divided the RMS difference columns in tables 6 and 8 by a factor of $\sqrt{2}$.

Table 6. Average and r.m.s values of the differences in photometric results between the two 7 μm exposures of stars in NGC 6522.

Range in 7 μm mag	No. of stars	Average difference	RMS difference
5–6	1	-0.17	0.17
6–7	13	-0.008	0.21
7–8	43	0.097	0.18
8–9	113	0.111	0.22
9–10	160	0.097	0.17
10–11	33	-.006	0.15

Table 7. Stars within the ISOGAL Sgr I field known to be long-period variables

ISOGAL no.	Lloyd Evans no.	Period days[1]	Differences[2]
514	39	336:	-0.15
363[3]	53	480	-0.42
511	54	293	-0.38
576	55	330:	-0.33
689	56	235	-0.31
684	57	153	-0.41
78	65	237	0.55
247[4]	79	383	0.34
402	87	308	0.16

Notes:
A colon denotes uncertainty in the period.
[1]Periods taken from Glass et al (1985) except for ISOGAL no. 576 which is from Lloyd Evans (1976).
[2]Between the two measurements in LW2. See also table 8.
[3] = IRAS17559-2901
[4] = IRAS17558-2858

Table 8. Average and r.m.s values of the differences in photometric results between the two 7 μm exposures of stars in Sgr I.

Range in 7 μm mag	No. of stars	Average difference	RMS difference
4–5	1	0.06	0.06
5–6	3	-0.010	0.34
5–6	1[1]	-0.22	0.22
6–7	16	-0.010	0.15
6–7	11[1]	-0.001	0.14
7–8	78	-0.030	0.17
7–8	76[1]	-0.020	0.14
8–9	157	-0.020	0.17
9–10	219	-0.017	0.17
10–11	43	-0.12	0.24

[1]When known variables are omitted.

3.4 OH/IR Catalogues

No known OH/IR sources fall within our fields (of 0.063 square degrees each). The density of known OH/IR sources in the part of the sky occupied by our two fields is only 1–2 per square degree (Sevenster et al., 1997), though it is higher at the Galactic Centre (∼10 per square degree for a survey of similar depth). The deepest surveys of the Central region indicate that the density of OH/IR stars reaches several hundred per square degree or about 1/3 the number of known large-amplitude variables (Glass et al., 1999). From their H_K colours, the Central region sources do not necessarily possess optically thick dust shells at K. However, it is not clear whether a deeper OH survey of the NGC 6522 and Sgr I fields would yield detections from the objects with moderate dust shells reported here.

4 THE ISOGAL [7]–[15], [15] COLOUR-MAGNITUDE DIAGRAMS

Stars detected at both wavelengths are shown in the [7]–[15], [15] colour-magnitude diagrams (Figs 8 and 9). The fact that these and similar diagrams discussed below show well-defined sequences implies that they are not significantly contaminated by foreground stars.

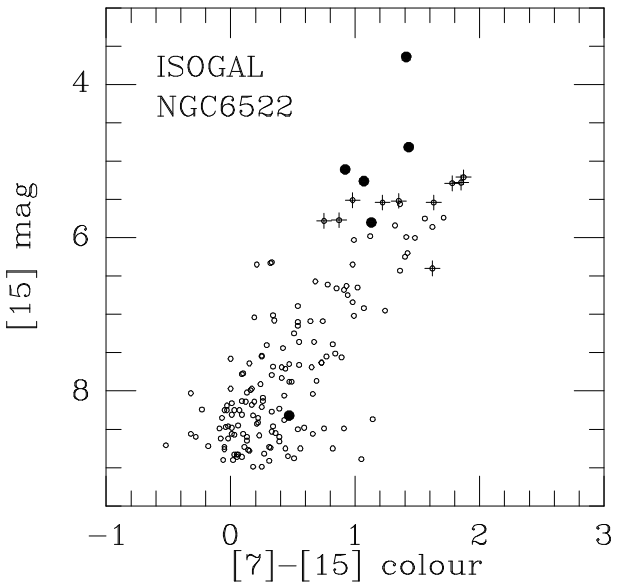

Figure 8. ISOCAM colour-magnitude diagram for the 15 × 15 arcmin^2 field in the NGC 6522 Window. Note that many sources are detected only at 7 μm and do not appear here. Known Mira variable stars are indicated by heavy points and some other stars chosen for investigation as possible high mass-loss objects are crossed. The [7]-[15] colours make use only of the second LW2 exposure, which was nearly simultaneous with the LW3.

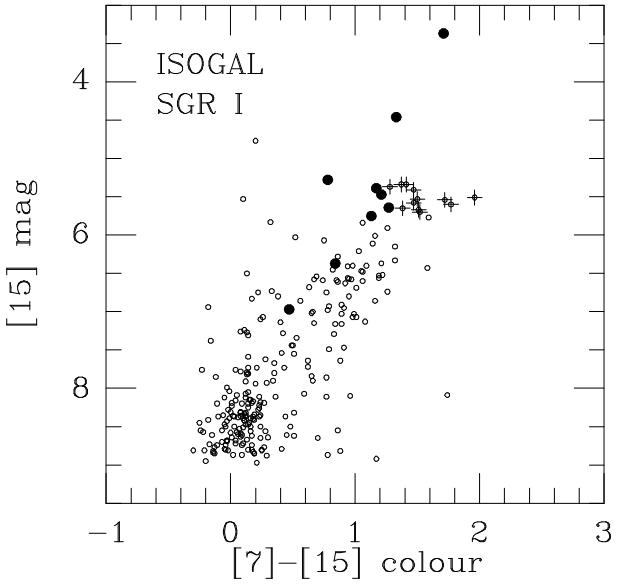

Figure 9. ISOCAM colour-magnitude diagram for the 15 × 15 arcmin^2 field in the Sgr I Window. See caption of fig. 8 for further details.

It is instructive to see how the [7]–[15] colours change with spectral type, bearing in mind that the few Miras may vary between late types. This is shown for the NGC 6522 field in Fig. 10, which includes all our sources that have been classified by BMB (1984) or Blanco (1986) and have been detected in both bands. Note that the fraction of stars satisfying both these criteria is almost zero for the early M-types and almost one for the later. Except for M sub-types 6, 6.5 and 7, the numbers are small. This selection effect

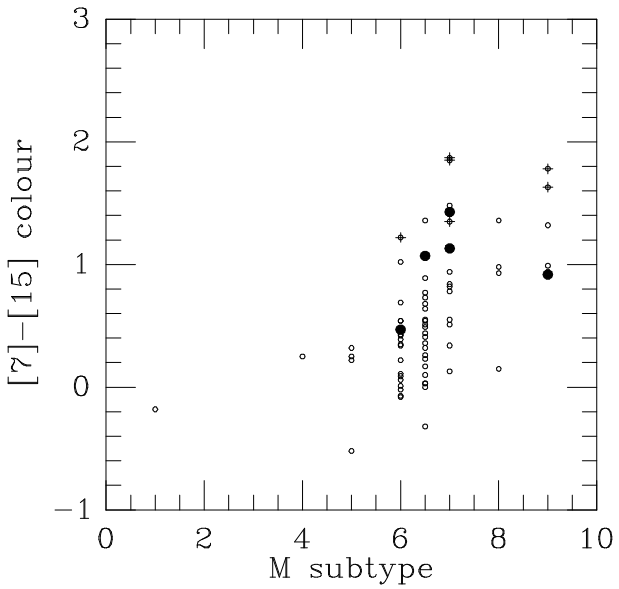

Figure 10. [7]–[15] colours vs spectral type for all spectrally classified stars that were detected at both wavelengths. The heavy dots are known Mira variables. Other high mass-loss objects are crossed. See text for discussion of selection effects. In calculating the colours only the second LW2 exposure was used.

arises from the fact that many stars fall below our limit in the 15 μm band.

4.1 Mira [7]–[15] colours

The [7]–[15] colours of the Mira variables are noticeably displaced from the extrapolation of the sequence formed by the remainder of the late M-stars in the ISOCAM colour-magnitude diagrams (Figs. 8 and 9). For Miras, the relative flux in the 7 μm-band must be greater or that in the 15 μm-band must be weaker or both.

O-rich Mira spectra have strong peaks due to the 9.7 μm and 18 μm silicate dust emission features. These are seen clearly in ISO-SWS spectra (Onaka et al., 1998). The ISOCAM LW3 band (12–18 μm) is situated longward of the 9.7 μm silicate band but is strongly influenced for about half of its width by the 18 μm feature. So far as is known, the LW3 band is not affected significantly by (gaseous) molecular absorption, the most conspicuous feature being the CO_2 band at 15.0 μm, which appears in some O-rich Miras (Onaka et al, 1997) with small equivalent width. In many sources an extension of the 10 μm peak to 13 μm, attributed to Al_2O_3, may also contribute to the ISOCAM 15 μm band.

5 K–[15] COLOURS

The K–[15] colour is primarily a measure of the infrared excess emitted by circumstellar dust shells. The K-band flux originates in the stellar photosphere and is only moderately affected ($\leq$ 0.1–0.2 mag overall) by CO and H_2O absorption bands. As mentioned above, the ISOCAM LW3 band (12–18 μm) is strongly influenced for about half of its width by the 18 μm silicate feature.

Here we consider those sources detected at 15 μm which

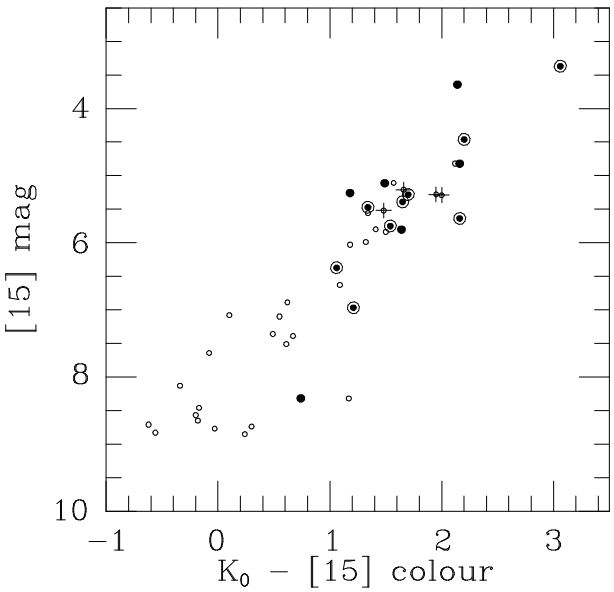

Figure 11. 15 μm mag vs K_0–[15] for a subset of stars in the NGC 6522 field detected at 15 μm and observed (not simultaneously) at K by Frogel and Whitford (1987). Mira variables are indicated by heavy points. Other high-mass-loss stars are crossed (see below). For convenience, the Miras in Sgr I (with K photometry from Glass et al., 1995) are also plotted (circled points).

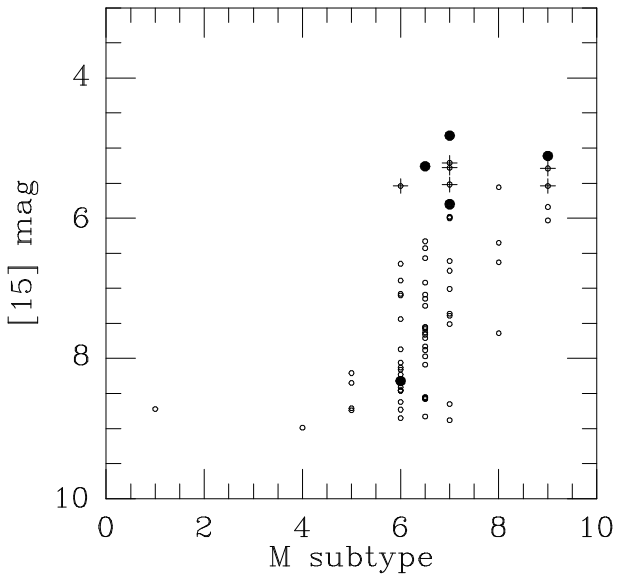

Figure 12. 15 μm mag vs M subtype for a subset of stars in the NGC 6522 field with 15 μm detections and spectroscopic information available. Symbols as in previous figure.

also have ground-based near-infrared observations available from Frogel and Whitford (1987). Spectral classifications by BMB (1984) or Blanco (1986) are also available for these objects. Figure 11 shows their 15 μm mag vs K–[15] colour and Fig. 12 shows the 15 μm vs M-subtype diagram.

There is a well-defined sequence of increasing 15 μm luminosity with K_0–[15] colour. Figs 11 and 12, as well as the other C-M diagrams, show that there is a steady increase of mass-loss from at least the mid-M giants to the Miras. It is also clear, for example by adding up the fluxes from each 15 μm magnitude band, that the flux from non-Miras exceeds that from the Miras. It is therefore also likely that at least half of the mass being returned from the stars to the interstellar medium is from the non-Miras.

As pointed out by Omont et al (1999c, in preparation), $K_0 \sim 8.2$ corresponds to the tip of the red giant branch (RGB)(Tiede, Frogel and Terndrup, 1995). This point corresponds (Fig. 11) to K_0–[15] ~ 0 or [15] ~ 8.2. Thus stars brighter than [15] ~ 8 are on the AGB.

6 HIGH MASS-LOSS OBJECTS WITH LITTLE OR NO VARIATION

Five of the known long-period variables in the NGC 6522 field are near the top of the ISOCAM colour-magnitude diagram (Fig. 8), but are interspersed with other stars that appear similarly luminous and somewhat redder. Ten of the latter stars, brighter than [15] = 5.7, were selected for detailed investigation. They are denoted by letters in Table 2 and are visible as red stars on V and I plates (Lloyd Evans, 1976). They have been re-examined for variability. Although BMB (1984) assigned very late spectral types and suggested variability, none of the ten stars is, in fact, a large-amplitude variable. However, variability with small amplitude cannot be excluded in about half of them. They therefore represent a type of late M-star with high mass loss but small or zero amplitude of variation. The colours of four of these stars (A, C, D and F) are shown in the $(J-K)_0$, K_0 diagram, Fig. 7, where they appear to be similar to 200–300 day Miras. One of the sample (star B) may be mainly at maximum, with occasional faint episodes, while stars A and G could be variables with occasional bright episodes superimposed on a constant background. Such variability in these stars is consistent with differences at 7 μm between the two observations, especially for star G (where the change amounts to ~ 0.53 mag).

For Sgr I, as in the case of the NGC 6522 field, 12 objects with 15 μm mags similar to the known Miras and somewhat redder colours were checked for variability by Lloyd Evans on the plate material. In all cases, these objects could be identified with very red stars. Only two were found to be fairly certain variables of low amplitude (F and H). Both these stars spend most of their time at maximum, with two fainter episodes separated by about 250 days for F and a single one for H.

The positions of these objects in the [7]–[15], [15] diagram (Figs. 8, 9) suggest that they form a continuation of the general sequence of late M stars and are not similar to the Mira variables. Unfortunately, only four of them, BMB 28, BMB 46, BMB 86 and BMB 179, have been measured in the near-infrared. Their K_0–[7] indicies are near-zero (Fig. 14).

Two of these non-Mira high mass-loss objects have been classified spectroscopically by BMB (1984) as M9, a spectral type that is usually associated with large-amplitude variability. It is known that the onset of Mira-type behaviour occurs at later types with increasing metallicity. The existence of this class of stars may therefore be a consequence of super metal richness. Alternatively, variability may have ceased temporarily but the dust shells have not yet dissipated.

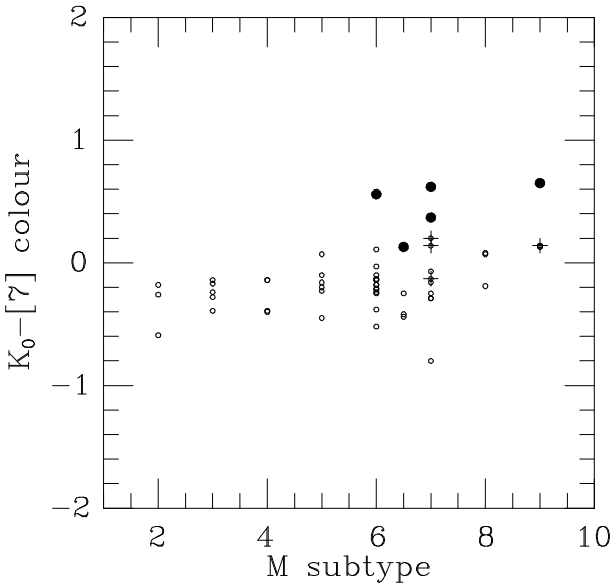

Figure 13. K_0–[7] colours vs spectral type for NGC 6522 field stars that have K_0 photometry by Frogel and Whitford (1987) and spectral classifications by BMB (1984) or Blanco (1986). This colour index is predominantly negative for unreddened M giants, except for some of the latest spectral types. Note the K and 7 μm photometry was not simultaneous, and that averaged 7 μm mags were used when available. Miras are shown as heavy dots and other high mass-loss objects are crossed.

Sloan and Price (1995) and Sloan, LeVan and Little-Marenin (1996) have shown that certain irregular and semi-regular AGB variables have dust excesses in IRAS spectra and are associated with the appearance of the 13 μm dust feature. By obtaining mid-infrared spectra for our objects or by obtaining more precise variability information it will be possible to decide if they are identifiable with this category. They may also be similar to the 'red' O-rich SRb variables of Kerschbaum and Hron (1996).

7 THE K_0–[7] COLOURS

The 56 objects of NGC 6522 with JHK photometry and spectral classifications are plotted in figure 13, which shows their K_0–[7] colours and spectral types.

These colours are unexpectedly negative in most cases, especially for the earlier M-subtypes. While part of this could be due to the small uncertainty in the absolute 7 μm photometry in crowded fields, ISO SWS spectra of late-type O-rich M stars frequently show a broad absorption shortward of the strong silicate dust peak at 10μm. This region is known to be affected by the SiO fundamental at $\sim$ 7.9 μm (Cohen et al., 1995). Carefully calibrated spectrophotometry of β Peg (M2.5 II–III) shows absorption at around 6 μm attributed to the ν_2 band of water vapour centred at 6.25 μm. Spectra of O-rich M-type giants that also demonstrate these features are presented by Tsuji et al. (1998), who envisage that they arise in a warm absorbing layer somewhat above the photosphere. Approximate calculations based on the Tsuji et al. spectra yielded K_S–[7] $\sim$ –0.1 for β Peg but slightly positive K_S–[7] for SW Vir (M7III)¶. The presence of significant amounts of dust could be an influence in the latter case.

The depth of the CO fundamental band in late M-type giants is known to have a similar effect on the $L-M$ colours, which tend to have low or negative values.

Figure 13 shows that in the latest M-type giants the K_0–[7] colour approaches zero or may even become positive. It is known that the overtone SiO absorption band at 3.95–4.1 μm is strong in semiregular variables but in Miras its strength varies with time and it can become weak (Aringer et al., 1995; Rinsland and Wing, 1982).

The optical depth of the circumstellar dust in the stars that we are discussing is very low in the earlier spectral types, rising somewhat towards the Miras but never becoming high. The emission at 9.7 and 18 μm is probably dominated by particles at a fairly uniform temperature around 1000 K, where condensation of silicate dust grains first becomes possible in the stellar wind. Thus the 15 μm fluxes are largely a measure of the mass of grains present and ultimately of the mass-loss rate from the star. The near-infrared K flux will not be affected by *emission* from the dust but will be reduced slightly by the *absorption* it causes at shorter wavelengths. The opacity of silicate dust at 7 μm is very low (see e.g. Schutte and Tielens, 1989) so that the trend of K–[7] colour with spectral type that we observe could partly be caused by increasing extinction at K and decreasing SiO and possibly H_2O molecular band strengths at 5.5–8 μm. However, dust emission at 7 μm is certainly responsible for the largest values observed in LPVs, as shown by Groenewegen (private communication) for various dust models.

7.1 The K_0–[7], [7] colour-magnitude diagram

In the K_0–[7], [7] colour-magnitude diagram (Fig. 14) we include the Miras from both fields. It is seen that almost all of the Miras are brighter and redder at 7 μm than the other red giants. A diagram involving the K_0–[7] colour will therefore be the best criterion for detection of large-amplitude LPVs.

8 ABSENCE OF VERY LUMINOUS SOURCES

Let us recall that, for the class of sources that we detect, the K bolometric magnitude correction is practically constant ($\sim$ 3.0; Groenewegen, 1997). With a distance to the Galactic Centre of 8.5 kpc, $M_{\rm Bol} \sim K_0$ - 11.65. The brightest stars in our fields therefore have bolometric magnitudes $>$ –5.9. Neither field includes any luminous dust-enshrouded AGB sources of the type found in the Large Magellanic Cloud by Wood et al. (1992), which reach luminosities of $M_{\rm Bol} \sim$ –7.5.

9 MID-INFRARED PERIOD-COLOUR RELATION FOR MIRAS

The Mira variables show a clear period-colour relation with very moderate scatter in the mid-infrared (Fig. 15). The [7]

¶ Spectrophotometry shows that $K - K_{DENIS}$ should have values of 0.02 to 0.07 for Miras because the K_S band does not include the first overtone band of CO.

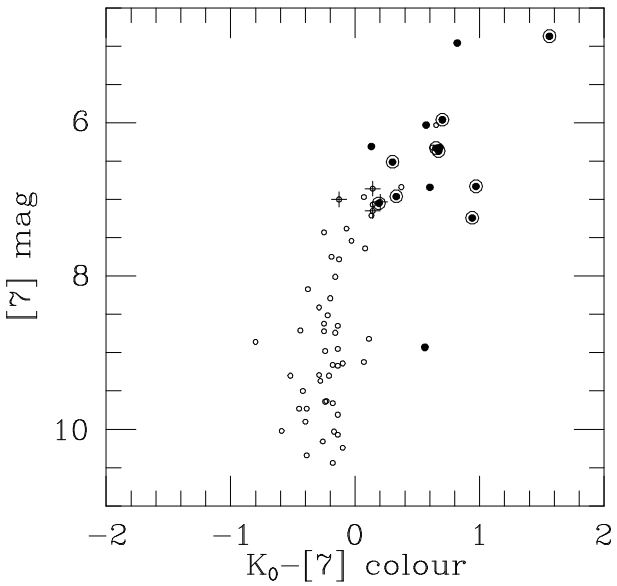

Figure 14. The K_0–[7], [7] colour-magnitude diagram, including Miras from NGC 6522 (heavy dots) and Sgr I (circled). The Miras are almost completely distinguishable from other stars by their bright 7 μm mags. Note that the K and 7 μm photometry was not simultaneous and that averaged 7 μm mags were used when available. Crosses denote other high mass-losing objects.

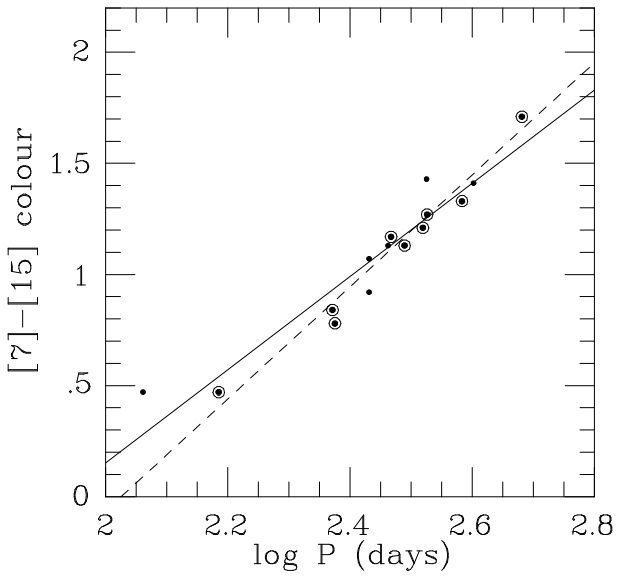

Figure 15. Mid-infrared period-colour relation for Mira variables, based on the Miras in the NGC 6522 (points) and Sgr I fields (circled points). The full regression line (solid) follows the equation [7]–[15] = 2.10 log P – 4.05. The rms differences between the fit and the observed points is 0.12 mag, rather better than expected from the photometric errors. If the shortest-period point is omitted, the fit (dashed line) becomes [7]–[15] = 2.52 log P – 5.11, with rms difference = 0.07. Only the second 7 μm exposure was used in forming the colours.

and [15] photometry is almost simultaneous, so that such scatter as exists is not attributable to variation between measurements. Following the discussion in section 7, this relation confirms that the mass-loss rate in Miras is directly related to their periods (see e.g., Whitelock et al., 1994).

The colour-magnitude diagrams for each of our two fields do not appear to contain any stars brighter than the known Miras. It is therefore likely that the census of stars at the long-period end of the the range is complete and that there is no evidence for long-period variables in our fields with periods longer than those already known, i.e. $\sim$ 700 d (see Glass et al., 1995).

10 STAR COUNTS

Determination of the spatial density distributions of the various stellar populations in the central Galaxy, and especially the bulge, is one of the key scientific goals of the ISOGAL project. A detailed analysis, covering several fields, and with careful consideration of completeness, extinction, etc, is in preparation. For the present we consider simply the differential number counts between the two fields at magnitudes above the completeness limit. At [15] this covers the AGB above the RGB-tip, while at [7] the limit extends approximately one mag below the RGB tip, to [7]$\sim$ 9.5, using K – [15] and K – [7] colours from Figs 11 and 14 respectively.

The ratio of the surface density of sources is, within the sampling errors, identical for both RGB and AGB stars, indicating that there are no steep population gradients apparent. It is also identical at both [7] and [15] microns. The surface density ratio is

$$\rho(\mathrm{Sgr\ I})/\rho(\mathrm{NGC\,6522}) = 1.85.$$

This count ratio corresponds to an exponential scale height of 2.0°, or $\sim$ 280 pc. That is, the inner bulge minor axis scale height is the same as that of the Galactic disk.

A more interesting comparison is with the scale height derived from analysis of the COBE/DIRBE surface brightness observations of the inner Galaxy. These have been analysed most completely by Binney, Gerhard, and Spergel (1997), whose best-fit model has a bulge density distribution which is a truncated power-law:

$$f_b = f_0 \frac{\mathrm{e}^{-a^2/a_m^2}}{(1 + a/a_0)^{1.8}}$$

with a_m=1.9kpc, a_0=100pc, f_0 a normalisation constant, and $a = (z/\xi)$ for $(x = y = 0)$, where z is the minor axis distance and ξ an axial ratio, with $\xi = 0.6$ best fitting the data. This density profile, which interpolates between the central luminosity spike, which follows an $R^{-1.8}$ luminosity profile, and the outer bulge, which follows an $R^{-3.7}$ profile, is also used in the models of Kent, Dame and Fazio (1991) and the kinematic analysis of Ibata and Gilmore (1995). It is known to provide an acceptable description of the bulge from latitudes of 4° to at least 12°. It remains to be tested at intermediate latitudes.

Direct comparison of the ISOGAL data with this function is of specific interest, since the fields surveyed here are included in the COBE/DIRBE analysis, and are of low reddening. The COBE/DIRBE data are however integrated light, and so must have a statistical correction for the foreground disk. This can be a complex function of wavelength and spatial resolution, especially at low latitudes (see Unavane et al., 1998, and Unavane and Gilmore, 1998) for a more complete description). Our ISOGAL source counts are however strongly biased against the foreground disk, being

dominated by sources in the central Galaxy. Thus, the ISOGAL observations test directly the analysis of the integrated light. Our present analysis however does not consider line of sight depth effects in the bulge itself.

With the adopted vertical axis ratio $\xi = 0.6$ the predicted count ratio in the ISOGAL data is $\rho(\mathrm{Sgr\ I})/\rho(\mathrm{NGC\,6522}) = 2.04$, somewhat larger than the observed value. Interestingly, near-exact agreement with the model above follows with an axis ratio $\xi = 1.0$, which predicts $\rho(\mathrm{Sgr\ I})/\rho(\mathrm{NGC\,6522}) = 1.81$. This systematic discrepancy between the model and our data is in agreement with the small systematic residuals emphasised to exist by Binney et al. (1997) and shown in their figure 2.

11 CONCLUSIONS

Most of the detected objects are late-type M stars, with a cut-off for those earlier than about M3–M4.

There is a continuous sequence of increasingly mass-losing objects from the mid-M-type giants to the long-period Miras, which are the most luminous stars in the field.

There appears to be no component of dust-enshrouded very long-period OH/IR stars or similar objects faint even at K in these fields. The upper limit of luminosities remains at $M_{\mathrm{Bol}} \sim -5.7$ and the upper limit of periods remains at about 700 days, as determined from near-infrared studies (Glass et al., 1995).

There is a group of late-type M-stars on the AGB which are not large-amplitude variables but may be irregular or of small amplitude, that have luminosities similar to Mira variables in the 200–300 day period range and show redder [7]–[15] but bluer K_0–[7] colours.

The ISOCAM 7 μm band is almost certainly affected by molecular absorption in ordinary M-giant stars. However, Mira variables are brighter than other stars possibly in part because of reduced SiO and H_2O absorption.

The results from these fields should form a template for analyses of more heavily obscured regions about which little is known from visible-light studies.

12 ACKNOWLEGMENTS

We would like to acknowledge the Les Houches 1998 summer school for access to the JUN98 version of CIA. We acknowledge useful discussions with K.S. Krishnaswamy, TIFR. Eric Copet is thanked for his help with the Unix scripts and Martin Groenewegen for his comments on dust at 7 μm. ISG wishes to acknowledge the hospitality of IAP during part of this work. SG and MS acknowlege receipts of fellowships from the Ministere des Affaires Etrangères, France, and ESA respectively.

REFERENCES

Abergel A., Miville-Deschênes M.A., Désert F.X., Pérault M., Aussel H., Sauvage M. 1998 http://www.iso.vilspa.esa.es/users/expl_lib/CAM_list.html

Alard et al. 1999, in preparation

Aringer B., Wiedemann G., Käufl H.U., Hron J. 1995, Ap Sp Sci, 224, 421

Binney J.J., Gerhard O.E., Spergel D.N. 1997, MNRAS 288, 365

Blanco V.M. 1986, AJ, 91, 290

Blanco V.M., McCarthy M.F., Blanco B.M. 1984, AJ, 89, 636 (BMB)

Blommaert J.A.D.L. 1998, *ISOCAM Photometry Report*, http://www.iso.vilspa.esa.es/users/expl_lib/CAM_list.html

Cesarsky C.J. et al. 1996, A&A, 315, L32

Cohen M., Witteborn F.C., Walker R.G., Bregman J.D., Wooden D.H. 1995, AJ 112, 241

Feast M.W. 1985, *Light on Dark Matter*, Israel F.P., Reidel, Dordrecht, p. 339.

Frogel J.A., Whitford A.E. 1987, ApJ, 320, 199

Ganesh S. et al. 1999, in preparation

Glass I.S. 1986, MNRAS 221 879

Glass I.S. 1993, *IAU Symp. 153: Galactic Bulges*, Habing H., Dejonge H., Kluver, Dordrecht, p. 21

Glass I.S., Feast M.W. 1982 MNRAS, 198, 199

Glass I.S., Matsumoto S., Carter B.S., Sekiguchi K. 1999 *IAU Symp. 191, Asymptotic Giant Branch Stars*, Le Bertre T., Lèbre A., Waelkens C., PASP Conf Ser, in press

Glass I.S., Whitelock P.A., Catchpole R.M., Feast M.W. 1995 MNRAS, 273, 383

Groenewegen, M. 1997, in *The Impact of Large-Scale Near-IR Surveys*, Garzon F. et al., Kluwer, p. 165

Ibata R.A., Gilmore G. 1995, MNRAS 275, 605

Kent S.M., Dame T., Fazio G. 1991, ApJ 378, 131

Kerschbaum R., Hron J. 1996, A&A, 308, 489

Lloyd Evans T. 1976, MNRAS, 174, 169 (TLE)

Ojha D., Omont A., Simon G. 1997, *IAU Symposium 184: The Central Regions of the Galaxy and Galaxies*, Sofue Y., p. 43

Omont A. and the ISOGAL Collaboration 1999a, to appear in *Astrophysics with Infrared Surveys: A Prelude to SIRTF*, Proc. First SIRTF Conf., Bicay M., PASP Conference Series

Omont A. et al. 1999b, to appear in *The Universe as seen by ISO*, Cox P., Kessler M.F., ESA Special Publications Ser. (SP-427)

Omont A. et al. 1999c, in preparation

Onaka T, Yamamura I., de Jong T., Tanabé T., Hashimoto O., Izumiura W. 1998, Ap Sp Sci, 255, 331

Onaka T., de Jong T., Yamamura I., Tanabé T., Hashimoto O., Izumiura W. 1997, Proc. First ISO Workshop on Analytical Spectroscopy, ESA-SP-419

Pérault M., Omont A. et al. 1996, A&A, 315, L165

Rinsland C.P., Wing R.F. 1982, ApJ, 262, 201

Sadler E.M., Rich R.M., Terndrup D.M. 1996, AJ, 112, 171

Schutte W.A., Tielens A.G.G.M. 1989, ApJ, 343 369

Sevenster M.N., Chapman J.M., Habing H.J., Killeen N.E.B., Lindqvist M. 1997, A&AS, 122, 79.

Sharples R., Walker A., Cropper A. 1990, MNRAS, 246, 54

Sloan G.C., LeVan P.D., Little-Marenin I.R. 1996, ApJ 463, 310

Sloan G.C., Price S.D. 1995, ApJ 451, 758

Stanek K.Z. 1996, ApJ 460, L37.

Tiede G.P, Frogel J.A., Terndrup D.M. 1995, AJ, 110, 2788

Tsuji T., Ohnaka K., Aoki W., Yamamura I. 1998, Ap Sp Sci 255, 293

Unavane M., Gilmore G. 1998, MNRAS 295, 145

Unavane M., Gilmore G., Epchtein N., Simon G., Tiphene D., deBatz B. 1998, MNRAS 295, 119

Whitelock P., Menzies J., Feast M., Catchpole R., Marang F., Carter B. 1994 MNRAS 276 219

Wood P.R., Whiteoak J.B., Hughes M.G., Bessell M.S., Gardner F.F. Hyland A.R. 1992, ApJ 397, 552